Advances in SQUID-detected magnetic resonance force microscopy

Wit, M. de

7

Dissipation of the alternating magnetic field source

Concerning the operation of a Magnetic Resonance Force Microscope at milliKelvin temperatures, one of the main challenges is the induced dissipation while creating the radio-frequency field necessary to manipulate the spins. Even though we use a superconducting RF wire, we still measure a significant dissipation which limits the ultimate operating temperature, the source of which remains unidentified. In this chapter, we present our attempt to shed some light on this problem, by carefully characterizing the amplitude- and frequency-dependent dissipation, and discussing a variety of possible sources.

7.1 Introduction

One of the crucial components of the MRFM setup is the source used to generate the B_1 field, which is necessary to manipulate the spins in the sample. There are two main approaches to making the microwave source. The first is based on (superconducting) microwave resonators, whose high quality factors amplify the generated magnetic fields, but at the cost of a limited bandwidth [63]. Alternatively, one can use an RF current passing through a microwire, allowing a larger operating bandwidth, but large currents are required to generate sufficient fields.

When operating an MRFM at low temperatures, it turns out that the dissipation of the RF source is the main limiting factor. For instance, Poggio et al. [57] generated a 4 mT field at the location of the sample by passing 20 mA through a copper microwire at a current density of $\sim 10^7$ A/cm^2. However, in doing so, they had a dissipated power of 350 μW. When measuring in a dilution refrigerator with a cooling power of only several μW at the mixing chamber at 15 mK, this is unacceptable. Therefore, our setup uses a superconducting microwire made of NbTiN in order to reduce the dissipation [49]. However, even when using a superconducting RF source an increase in sample temperature is observed during pulses. As a varying sample temperature strongly affects an MRFM measurement (i.e. by changing the Boltzmann polarization of the spin ensemble or inducing shifts of the resonance frequency and quality factor of the cantilever), it is paramount to solve this issue.

In this chapter, we investigate the dissipation when sending alternating currents through our RF microwire by using our MRFM setup as a calorimeter. We then compare this measured dissipation to various possible mechanisms which could cause dissipation due to an alternating current. In doing so we try to understand the origin of the dissipation and, hopefully, find a solution to this longstanding problem.

7.2 Calorimetry at mK temperatures

7.2.1 Cryogenic dual-compensated calorimeter

In order to measure the dissipated power at low temperatures, we use our MRFM setup as a dual compensated calorimeter. The operating principle of such a calorimeter is shown in Fig. 7.1. The idea is straightforward: two temperature controllers are

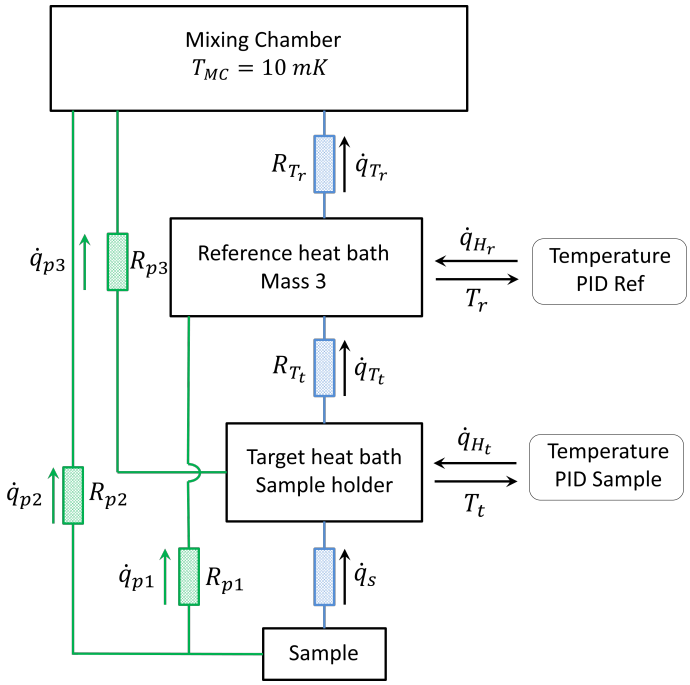

Figure 7.1: Schematic of the operation principle of a dual compensated calorimeter. The blue parts parts indicate the intended heatlinks between the different calorimeter stages, while the parts in green are parasitic thermal connections. A dual temperature controller maintains both the target and reference heat bath at constant temperatures.

used to hold the target (T_t) and reference (T_r) heat baths at a constant temperature, with T_t slightly above T_r. The total heat flow to and from the target heat bath is given by:

$$\dot{q}_{H_t} = \dot{q}_s - \dot{q}_{\mathrm{T_t}} - \sum_n \dot{q}_{pn} \tag{7.1}$$

where $\dot{q}_s$ is the power from the sample that reaches the target heat bath, $\dot{q}_{\mathrm{T_t}}$ the heat flow from the target to the reference heat bath, $\dot{q}_{\mathrm{H_r}}$ the power used by the temperature controller to maintain constant temperature, and $\dot{q}_{\mathrm{pn}}$ are all parasitic heat flows that bypass one or both of the heat baths. Because we keep T_t and T_r constant, all thermal conductivities of the various materials stay the same during the measurement. If we also assume that the sum of all parasitic heat losses is small and constant, we can directly measure the power dissipated on the sample, since this can be measured as a decrease of the control power required to keep the target heat bath at a constant temperature.

The measurement protocol depends on differential measurements of the required

heating power on the sample, with the reference bath always at a constant temperature. First, the reference power (P_1) required to keep the sample holder at a certain setpoint temperature is measured without any heating on the sample. Second, the reference power is switched off, and the target bath is allowed to cool down to the temperature of the reference bath. Third, dissipation on the sample is switched on, in our case by sending continuous RF power through the RF wire. When the temperature without feedback is stable, the temperature controller is switched on, and the new required power (P_2) to heat the sample holder to the temperature setpoint is determined. The power dissipated by the sample is now given by the difference between P_1 and P_2.

In reality, we did not use a dedicated calorimeter setup for the experiments presented in this chapter. Instead, we simply used the Fermat MRFM setup, where the sample holder is used as the target heat bath, while we use the bottom mass of the vibration isolation (mass 3) as the reference heat bath. The heat conductance between the two baths has been measured for different temperatures, the result of which is shown in Fig. 7.2. The linear dependency on the temperature matches electronic thermal conductance at low temperatures [109], while the magnitude of the measured value indicates that the conductance is limited by the brass screw used to connect the sample holder to the outer housing of Fermat: An M2 brass screw with a length of 1 cm would lead to a thermal conductance of approximately 10 nW/mK at a temperature of 100 mK. An AR3 low temperature thermometer[1] is used in combination with a 100 Ohm heating element to control the temperature between 15 mK and 1 K. The final achieved power resolution varies between 1 and 100 nW depending on the setpoint temperature of the sample holder, and the ferocity of the PID controller.

7.2.2 NbTiN RF wire

The RF wire under investigation in this chapter can be seen in Fig. 7.3(a), and consists of two leads with dimensions 2000 x 20 x 0.3 μm, and a constriction with dimensions 300 x 1.0 x 0.3 μm. The transition between the leads and the constriction has rounded corners to prevent current crowding which reduces the critical current [171]. It was fabricated according to the recipe outlined in appendix D, based on NbTiN films grown by David Thoen [55]. The superconducting properties of the RF wire were measured in a vacuum chamber inside a liquid helium dewar. A DC transport critical current of 28.3 mA was measured, equivalent to a critical current density of $9 \cdot 10^6$ A/cm^2 (see Fig. 7.3(b)). The residual DC resistance well below the critical current is less than 0.1 mΩ.

[1] Supplied by Hightech Development Leiden (HDL), calibrated range 10 mK - 1.1 K.

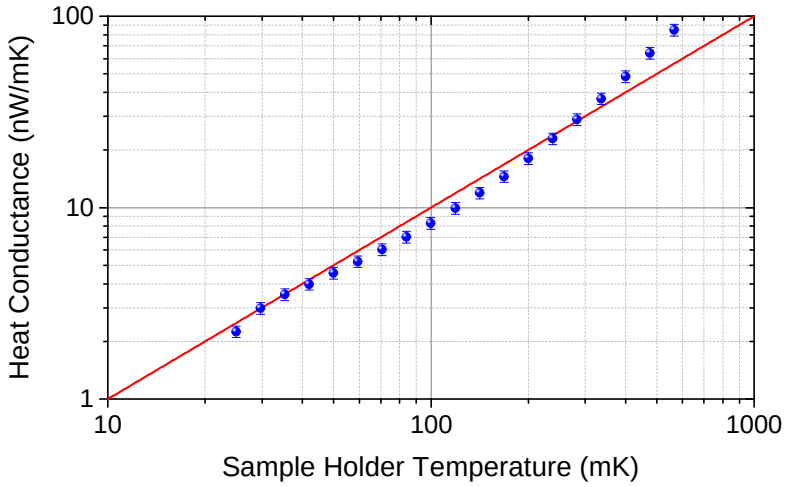

Figure 7.2: Thermal conductance between the sample holder and mass 3. The red line indicates the expected linear dependence between the heat conductance and temperature. The error bars are based on the uncertainties in the thermometer calibration and low temperature restistance of the heater.

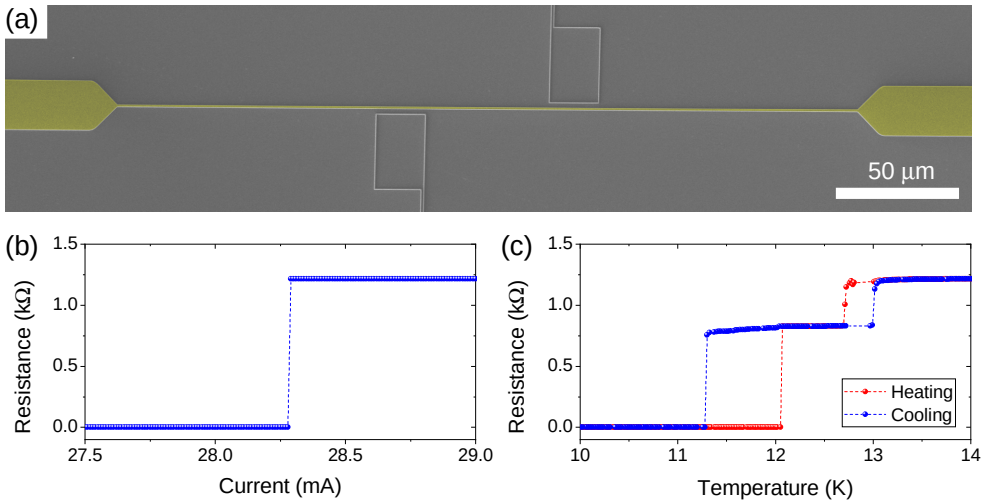

Figure 7.3: Properties of the RF wire under investigation. (a) Scanning electron microscope image of the RF wire (yellow), consisting of a narrow part with dimensions 300 x 1.0 x 0.3 µm, and two leads with dimensions 2000 x 20 x 0.3 µm. (b) Measurement of the critical current at 4.2 K and a pressure of $\sim 10^{-3}$ mbar. (c) Measurement of the critical temperature, where the red curve is measured during heating, and the blue curve is measured during cooling.

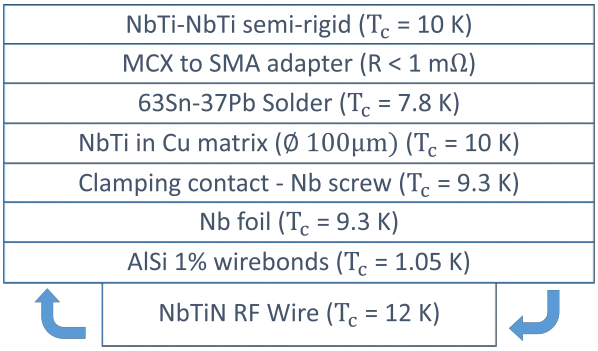

Figure 7.4: List of all components of the RF circuit from the mixing chamber (top) to the sample (bottom).

The superconducting transition temperature of the RF wire can be seen in Fig. 7.3(c). The two distinct steps correspond to slightly different critical temperatures for the constriction and leads of the RF wire, where the RF wire is responsible for the lower temperature step as surface impurities have more effect on narrow structures. The difference between heating and cooling is due to the thermal delay between the sample holder and the RF wire. We deem the heating curve to be more reliable, leading to a critical temperature of $\sim$ 12 K, slightly less than the value reported for the full wafer [55].

7.3 Characterization of dissipation

We have used the setup described in the previous section to measure the dissipated power in the RF wire for various (RF) currents. The most straightforward experiment is simply sending a direct current I in order to determine the resistance R in the system following a Joule heating model where $P = RI^2$. Fig. 7.5 shows the result of this experiment, where we observe a power dissipation of up to tens of nanoWatts, and where the red solid line represents the Joule heating model with a residual resistance of 0.9 mΩ. A residual resistance this low is nearly unavoidable in any circuit with transitions between materials, and in this case might be explained by, for instance, the oxide layer on the niobium at the clamping contact transition to the copper/NbTi wire (see Fig. 7.4).

When the direct current is replaced by an alternating current, Joule heating hardly changes. For an alternating current $I(t) = I_0 \cos(\omega t)$, the dissipated power is given

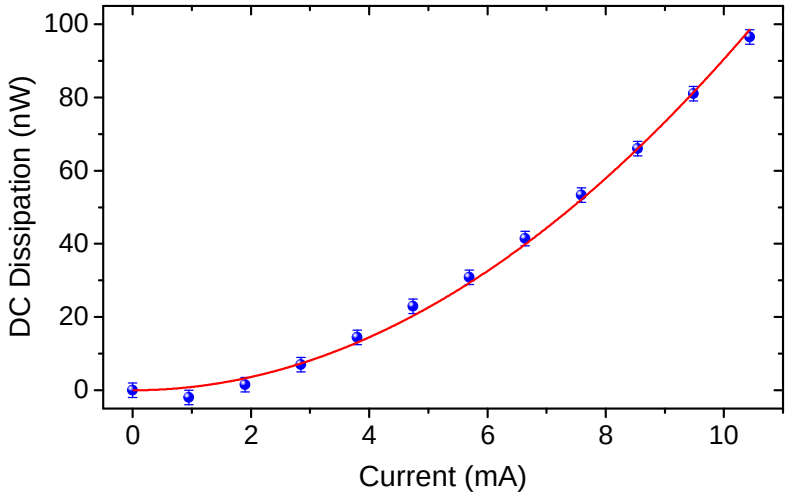

Figure 7.5: Measured disspation at the sample holder versus direct current. The red line is a parabolic fit to a simple Joule heating model with a residual resistance of roughly 0.9 mΩ. The error bars are estimated from the noise on the applied power.

by:

$$P(t) = RI^2(t) = RI_0^2 \cos^2(\omega t) = RI_0^2 \left(\frac{1}{2} + \frac{1}{2} \cos(2\omega t) \right) \tag{7.2}$$

Evidently, we obtain an oscillating power with an average of $P = RI_{\mathrm{rms}}^2$. This in turn would lead to a final temperature consisting of a constant temperature increase with respect to the surroundings, plus an alternating component oscillating with frequency 2ω. However, if this frequency is larger than the inverse thermal time constant of the system (e.g. the sample holder), this alternating component will be averaged out. What allows us to distinguish AC Joule heating from other effects, is that the Joule heating is independent of the frequency of the current. Therefore, when we measure the dissipation as a function of frequency, it should only show up as a dissipation background, equal at all frequencies.

In Fig. 7.6 we have measured the dissipation resulting from a 200 kHz alternating current with varying amplitude. The inset shows similar data, but measured at different (higher) frequencies (with an inferior power resolution). The solid lines are fits to the data to a model $P = c(f)I^2$. So, the dissipation scales in the same way as expected from Joule heating, but the magnitude of the measured dissipation is much larger than what was observed for DC in Fig. 7.5. Therefore, we have to look for an additional source of dissipation which seems to be dominant in our setup.

More insight on the matter might be obtained from the influence of the RF fre-

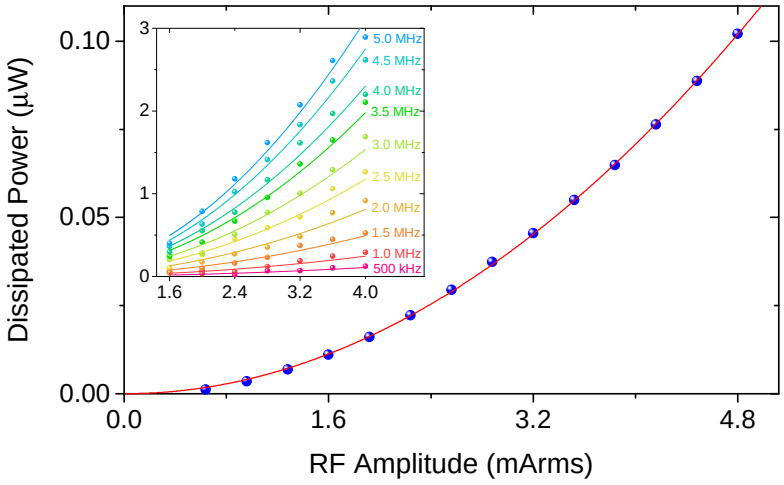

Figure 7.6: Dissipated power vs amplitude of the RF current at a frequency of 200 kHz at a sample holder temperature of 50 mK. The red line represents a quadratic relation between the amplitude and power. At 200 kHz, the dissipation is 4 times the DC dissipation. Inset: the same measurement at different RF frequencies and at a sample holder temperature of 70 mK.

quency. We have varied the RF frequency from 100 kHz to 20 MHz at a constant current of 1.6 mA_{rms}. The measured dissipation for all frequencies is shown in Fig. 7.7. Measurements were done at a sample holder temperature of 150 mK (blue), 300 mK (green), and 500 mK (orange). From the nice overlap between the different curves, we can conclude that the temperature does not influence the amount of power dissipated. The red solid lines are fits to a simple power law $P = cf^b$, with c a free fitting parameter, and $b = 0$, 1, and 1.5. We find that at low frequencies, the power scales linearly with the RF frequency, but as the applied frequency increases the dependency changes to $P \propto f^{1.5}$. The inset shows more measurements of the dissipated power vs frequency for different RF currents, but this does not seem to affect the measured frequency-dependence. The solid lines are fits to the data of a powerlaw with $b = 1.5$.

Let us summarize what we have learned from the experimental data in this section. The dissipation can be divided into an AC and DC component. The DC component corresponds to Joule heating over a 0.9 mΩ resistive component somewhere on or near the sample holder. The dissipated power from the AC component seems to be independent of temperature (for temperatures below 500 mK), and scales quadratically with the amplitude of the RF current. The frequency dependence of the dissipation seems to vary between $P \propto f$ and $P \propto f^{1.5}$, depending on the actual RF frequency. We can now use this data to speculate about the source of the (AC) dissipation.

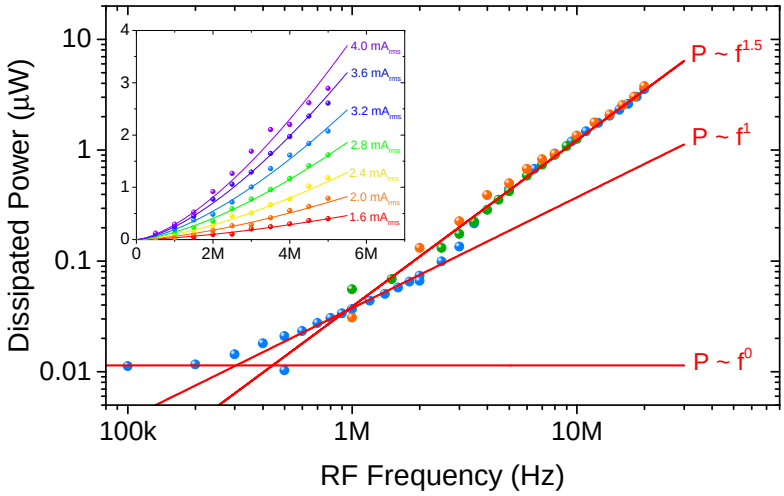

Figure 7.7: Dissipated power vs frequency of the RF current, measured at 1.6 mA_{rms}. The red lines indicate fits to a simple power law $P = cf^b$ for b = 0, 1, and 1.5. Data was measured at a sample holder temperature of 150 mK (blue), 300 mK (green), and 500 mK (orange). Inset: the same measurement but at different RF amplitudes, measured at 300 mK.

7.4 Models for the origin of dissipation

When looking for the origin of the dissipation in our RF wire, there are two main suspects: losses due to eddy currents in surrounding metals, and dissipation within the superconductor itself.

7.4.1 Eddy currents and skin effect

When a time-varying magnetic field is present in a conducting material, eddy currents are generated to compensate for the changing flux. As the conductivity of normal metals has a finite value, these eddy currents are subsequently dissipated into heat. In general, analytical calculations of eddy currents are complicated, but using the appropriate limits and approximations they are certainly possible [172]. An important concept is the skin depth which describes the attenuation of the free space magnetic field within a material [173]:

$$\delta = \sqrt{2\rho/\omega\mu}, \tag{7.3}$$

where ρ is the resistivity of the material, and ω is the angular frequency of the alternating magnetic field. μ is the magnetic permeability of the material, which we

will set equal to μ_0 since we only look at nonmagnetic materials. The precise value for the skin depth is difficult to calculate because often the low temperature resistivity of, e.g., copper is not known, since this depends on the residual resistivity ratio (RRR) of the particular copper component [174]. For the MHz frequencies we typically use in our MRFM experiments, the skin depth is of the order of 10 μm.

A particularly nice analysis is given by Meyer et al., who calculate the dissipated power due to eddy currents in two limits. If the thickness of a metal plate is much larger than the skin depth (the inductive limit, $d \gg \delta$), most eddy currents flow across the surface of the plate, and the dissipated power is given by: [115]

$$P = A\left(\frac{B_0}{\mu_0}\right)^2\left(\frac{\rho}{\delta}\right) \propto \sqrt{\omega\rho}, \tag{7.4}$$

where B_0 is the amplitude of the alternating magnetic field in free space, and A is the area of the plate. The opposite limit is when the metal plate is so thin compared to the skin depth that the plate practically becomes transparent to the field (the resistive limit, $d \ll \delta$). In that case the dissipation scales strongly with the thickness of the plate:

$$P = A\left(\frac{B_0}{\mu_0}\right)^2\left(\frac{d}{\delta}\right)^3\frac{\rho}{6\delta} \propto \frac{\omega^2 d^3}{\rho}. \tag{7.5}$$

We can use Eqs. 7.4 and 7.5 to check if eddy current dissipation is the main source of heating in our experiment by comparing the predicted and measured power laws. Note that these equations assume a varying magnetic field that is homogeneously distributed in free space, which is not the case in our setup where all magnetic fields are very local.

When looking at potential sources for eddy current dissipation in our setup, there are two likely candidates: a thin metallic sample right next to the RF wire, and the copper sample holder underneath the detection chip.

For a metallic sample with a thickness of 100 nm, we are in the resistive limit, so we can use Eq. 7.5 while taking into account that the magnetic field of the RF wire decreases with distance [2]:

$$P = l\left(\frac{1}{\mu_0}\right)^2\left(\frac{d}{\delta}\right)^3\frac{\rho}{6\delta}\left(\frac{\mu_0 I}{2\pi}\right)^2\int\frac{1}{r^2}dr, \tag{7.6}$$

where the integral is taken over the entire width of the sample, and l is the length of the sample along the RF wire. The resulting dissipation for the expected lower

[2] The magnitude of the magnetic field of a wire carrying a current I is simply given by $|B| = \frac{\mu_0 I}{2\pi r}$, with r the distance from the wire.

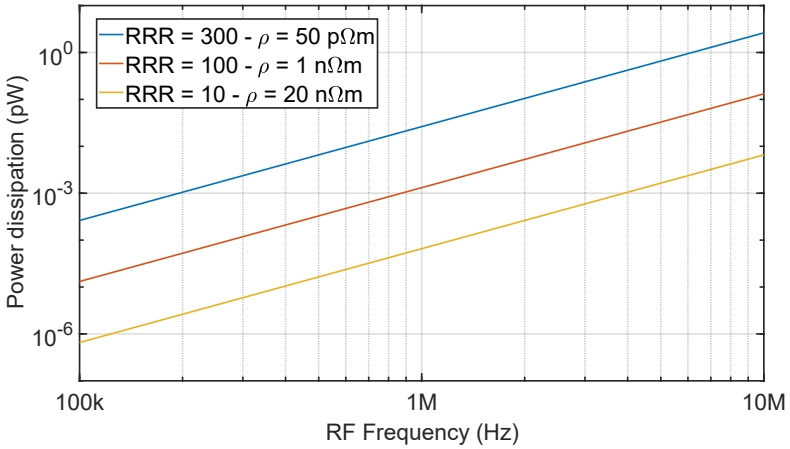

Figure 7.8: Calculation of the dissipation induced by eddy currents due to a 10 mA_{pk} current in the RF wire for a metallic sample of thickness 100 nm for different RRR values.

and upper limits of the RRR value of the copper is seen in Fig. 7.8. Even for pretty extreme parameters of a peak current of 10 mA_{pk} at a frequency of 10 MHz, the dissipation only reaches pW levels.

For eddy currents induced in the sample holder, we are well in the inductive limit. In this case we can modify 7.4 by once again taking into account the magnetic field distribution to calculate the dissipation:

$$P = \left(\frac{1}{\mu_0}\right)^2 \frac{\rho l}{\delta} \left(\frac{\mu_0 I}{2\pi}\right)^2 \int \frac{1}{(d^2 + r^2)} dr \tag{7.7}$$

Here d is the thickness of the detection chip (the minimal distance between the sample holder and RF wire), and the integral is taken over the full width of the sample holder. Once again, we have calculated the expected dissipation for typical RF pulse parameters, the result of which can be seen as the blue curve in Fig. 7.9. The red curve in this figure is the result of a finite element analysis using COMSOL Multiphysics for the same system with the same settings. Both methods show the same $\sqrt{\omega}$ dependency, and in absolute values they are within a factor of 2 of each other. The absolute value for the dissipation is between 10 and 100 nW, so the effects of eddy currents in the sample holder are certainly present, but are still small compared to the dissipation measured in the setup.

Based on these calculations, we conclude that both the frequency-dependence and absolute values of the eddy current losses indicate that they are not responsible for the observed dissipation during the MRFM experiments.

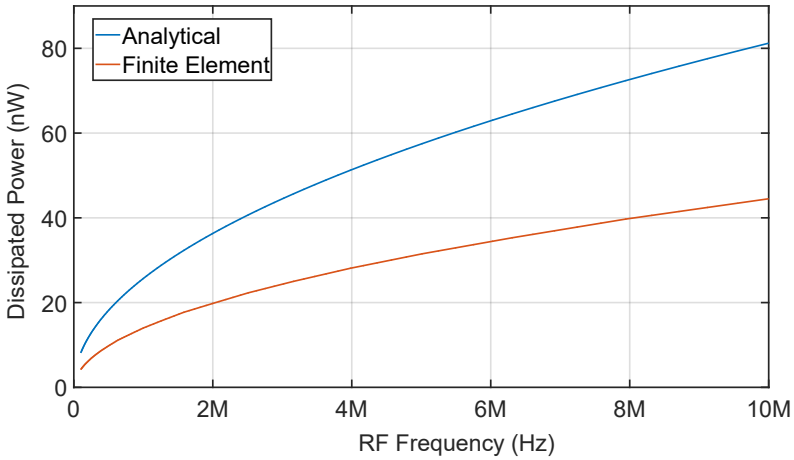

Figure 7.9: Calculation of the dissipation due to a 10 mA_{pk} current induced by eddy currents in the sample holder located 0.5 mm below the RF source, assuming a resistivity of 1 nΩm (RRR = 100).

7.4.2 Dissipation in type-II superconductors

A completely different line of thought is that the dissipation originates within the superconductor. We will consider two different mechanisms for losses in a superconductor carrying an alternating current. The first is based on the presence of quasiparticles in the superconducting condensate, and the second on the movement of flux vortices penetrating the superconductor. As we are only trying to identify potential origins of the dissipation, the theoretical description of these models will be minimal. For a more in-depth analysis, the reader is referred to more specialized work like Tinkham [175] and Annett [176].

The quasiparticle model: For high frequency currents, we can use the two-fluid model to predict that normal electrons (the quasiparticles) within the superconducting condensate can give rise to a finite amount of dissipation [175]. The normal and superconducting electrons can be seen as two parallel conduction channels, one resistive (dissipation) and one inductive (no dissipation), leading to a total conductivity given by

$$\sigma(\omega) = \sigma_1(\omega) - i\sigma_2(\omega), \tag{7.8}$$

with $\sigma_1 = n_n e^2 \tau_n / m$ the conductivity of the normal channel and $\sigma_2 = n_s e^2 / m\omega$ the conductivity of the superconducting one. τ_n is the scattering relaxation time of the normal electrons, and n_n and n_s are the densities of the normal and superconducting

electrons. At low frequencies, the inductive superconducting channel shorts the resistive one, but there is a crossover frequency above which the resistive channel becomes favourable. This crossover frequency is given by $\omega \approx (n_s/n_n)(1/\tau_n)$. This frequency is expected to be very high, due to the short τ_n, which is in the fs range [177], and due to the fact that in the BCS theory, $n_n \sim \exp(-\Delta/k_B T)$, so n_n goes exponentially to zero at low temperatures. However, even far below the crossover frequency, there will always be a nonzero dissipation from the normal component.

Following the argument above, given an imposed alternating current density J, the dissipation per unit volume is given by $Re(1/\sigma)J^2 = [\sigma_1/(\sigma_1^2 + \sigma_2^2)]J^2 \approx (\sigma_1/\sigma_2^2)J^2$, where we assumed $\sigma_1 \ll \sigma_2$. Inserting the conductivities for both channels, we find:

$$\mathcal{P} = \frac{n_n \tau_n m}{n_s^2 e^2} \omega^2 J^2 \tag{7.9}$$

Thus, the dissipation in this model should be proportional to the square of both the frequency and the amplitude of the AC current.

When we compare this model to the experiments described in this chapter, we find that the model matches in terms of the current-dependence of the dissipation. However, we do not observe a quadratic dependence on the frequency. Giving an actual number for the dissipation based on this equation is difficult, but since we measure at temperatures far below the energy gap of NbTiN ($\Delta \sim 1.76\ k_B T_c \approx k_B \cdot 26$ K) [55] we expect n_n to be extremely small, and thus the dissipation to be small as well. We therefore deem it unlikely that this is the main origin of the observed dissipation.

The vortex model: A defining property of type-II superconductors is their capability to carry supercurrents at relatively high magnetic fields. The explanation for this was given by Abrikosov, who hypothesized that quantized magnetic vortices are allowed to enter the superconductor when it is subjected to a magnetic field between the lower (H_{c1}) and upper (H_{c2}) critical field [178]. However, several theories are now holding these vortices responsible for the observed dissipation in superconductors. When a current density J is applied, a Lorentz force $F_L = \Phi_0 J$ acts on the vortex[3] [179]. Here $\Phi_0 = h/2e$ is the magnetic flux quantum. When this force is smaller than the pinning force holding the vortex in place, the vortex will make a small oscillation around its pinning site, similar to a particle trapped in a potential U_0. Thermally assisted flux creep is possible when the temperature $T \gg U_0/k_B$, but in our temperature regime it is estimated that this motion of vortices does not lead to significant

[3] Actually, this is the Lorentz force per vortex per unit length.

dissipation. This situation changes when the current density is increased and the Lorentz force becomes larger than the pinning force, in which case the vortices start to move [180]. This leads to the dissipation of energy, as experimentally observed by Raes et al. [181].

In the Bardeen-Stephen model for the case of free vortex flow without pinning it is assumed that the core of the moving vortex with radius ξ is fully normal[182]. Dissipation occurs due to ordinary resistive processes in the core. Following this model, it is found that the power dissipated per unit volume due to the flow resistance ρ_{f} is given by [179]:

$$\mathcal{P} = J^2 \rho_{\mathrm{f}} = J^2 \rho_{\mathrm{n}} \frac{B}{H_{\mathrm{c2}}}, \tag{7.10}$$

with $B = \Phi_0 / a_0^2$, where a_0 is the spacing between vortices. So, in the Bardeen-Stephen model, dissipation rises quadratically with the RF current. Note that the dissipation is a fraction B/H_{c2} of the dissipation in the normal state with resistance ρ_{n}. Additionally, as the origin of the dissipation in this model is a viscous flow of the vortex, the power dissipation is also quadratic with the velocity of the vortex, and thereby quadratic with the frequency of the RF current.

We can try to calculate an order of magnitude number for the dissipation due to the flux flow mechanism described above. For this, we calculate the upper critical field

$$B_{\mathrm{c2}} = \mu_0 H_{\mathrm{c2}} = \frac{\Phi_0}{2\pi\xi^2} \sim 20 \text{ T}, \tag{7.11}$$

where $\xi = 3.8$ nm is the BCS coherence length of NbTiN [183, 184] . When we assume that the vortices have entered the RF wire during cooldown in the earth's magnetic field, and that all losses occur within the narrow part of the RF wire, the dissipated power is on the order of 1 µW, which is definitely in the right ballpark.

As we measure an exponent of the frequency-dependence of the power dissipation between 1 and 1.5, it remains unclear via what mechanism the vortices induce losses. Anyway, the influence of vortices can be checked by applying a direct current in combination with the RF current. The idea here is that as soon as the field induced by the wire itself surpasses H_{c1}, additional vortices will enter the wire. The first critical field of the NbTiN can be calculated using [176]

$$H_{\mathrm{c1}} = \frac{\Phi_0}{4\pi\mu_0\lambda^2} ln\left(\frac{\lambda}{\xi}\right), \tag{7.12}$$

where $\lambda = 260$ to 300 nm is the London penetration depth [55, 185]. Using these values, we find a critical magnetic field $B_{\mathrm{c1}} = \mu_0 H_{\mathrm{c1}} \sim 8$ mT. The current necessary

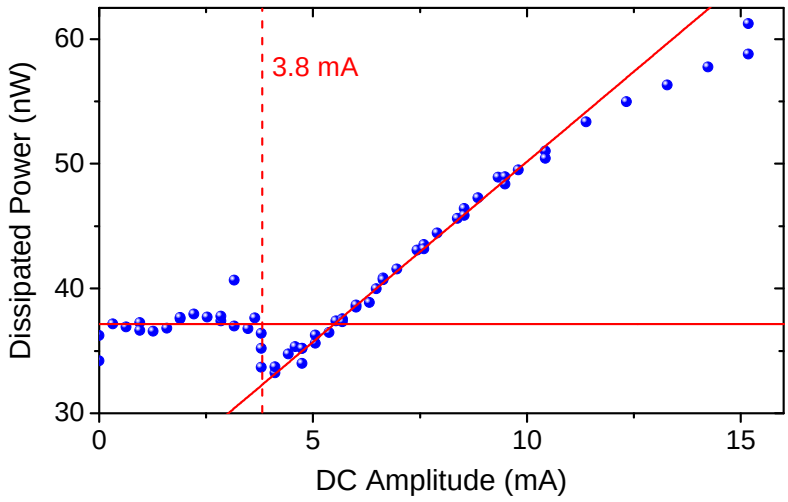

Figure 7.10: Measurement of the dissipation due to an RF current of 1.6 mA_{rms} at 1 MHz as a function of the applied direct current.

to create this field at the surface of a wire of radius R_0 is given by [175]

$$I_{c1} = \frac{2\pi R_0 B_{c1}}{\mu_0} \left(\frac{2}{3}\right)^{3/2}, \tag{7.13}$$

leading to a critical current of 3.3 mA. Here we assume the wire to be cylindrical with a diameter equal to the thickness (so $R_0 = 150$ nm). When the applied direct current gets above this value, the dissipation should increase linearly with the number of vortices, and thus with the amplitude of the direct current [186].

A direct current with a peak value of 50 mA was added to the RF current using a bias tee. After attenuation at the 4K plate of the cryostat, this leaves a current of up to 16 mA. To subtract the Joule heating, we again relied on differential measurements, where we first measure the dissipation with only the direct current, and subsequently with both the DC and AC at the same time. As can be seen in Fig. 7.10, indeed the measured dissipation stays constant up to a direct current of about 4 mA, after which it increases linearly with the applied current. The measurement was performed with an alternating current of 1.6 mA_{rms} at 1 MHz, with a sample holder temperature of 70 mK to optimize the power resolution.

Interestingly, coinciding with the onset of the linear increase in the dissipation is a distinct dip of roughly 5 nW. Possibly, this is caused by the transition from flux penetrating the edges of the RF wire to flux vortices which completely penetrate the superconductor, which might lead to a more favorable overall field distribution.

7.5 Suggestions to reduce dissipation

It has become clear that the dissipation observed in the MRFM RF wire can originate from a number of possible sources, where we estimate the effects of flux vortices to be dominant. In order to reduce the dissipation, there are several technical options to consider:

- Reducing the Joule heating: we have measured a residual resistance of 0.9 mΩ in our RF circuit, which we attribute to one or several of the transitions between different materials and to the connectors in the circuit. The residual resistance can be improved by replacing all clamping contacts by spotwelded connections [170], or by moving all connections as close to the mixing chamber as possible, where more cooling power is available to remove generated heat.

- Reducing eddy current losses: As we have seen, the largest part of eddy current losses is expected to be induced in the copper sample holder. Increasing the distance between the RF wire and metal components in the setup would reduce these losses. However, as the magnetic field generated by a wire falls off linearly with the distance to the wire, large separations are needed to get a significant improvement. This could be done by placing the detection chip on top of a sapphire sample holder. Alternatively, one could try to shield the normal metals from the magnetic field by coating the bottom of the detection chip with a layer of superconducting material with a thickness much larger than the London penetration depth. However, both of these options will probably reduce the thermalization of the sample.

- Reducing flux vortices losses: When we assume the movement of flux vortices to be responsible for the power dissipation, there are two things we can do. The first is to reduce the total number of vortices. Stan et al. have shown that the maximum field you can apply before vortices enter a thin superconducting strip is given by $B_\mathrm{m} \approx \Phi_0/w^2$, with w the width of the strip [186]. So, by reducing the width of the RF wire, the number of vortices at a given field can be reduced. The downside to this is that a narrow RF wire has a higher current density, which could enhance the flux flow of the remaining vortices, and reduces the maximal B_1 field. A similar effect can be achieved by making a laminar RF wire, where the thickness d of each layer is well below the London penetration depth. Then, the first critical field is enhanced via

$$H_{\mathrm{c1}} = \frac{2\Phi_0}{\pi d^2} ln\left(\frac{d}{\xi}\right), \tag{7.14}$$

which prevents vortices from entering [187]. The second approach is to enhance the pinning of the vortices, and thereby reduce vortex motion. This can be done by intentionally introducing defects in the superconductor [188–190] or applying the appropriate external magnetic fields [191, 192].

- Reducing dielectric losses: This is a topic we did not cover before, but it has been reported that the presence of the dielectric substrate, in our case the SiO_2, can cause dissipation in superconducting resonators [52, 193, 194]. It is not clear if this type of dissipation is currently an issue in our RF wire. As a precaution, it might be possible to etch away the substrate near the RF wire to create a trenched microwire. Removing the dielectric from areas with high electric field gradients has been shown to improve the performance of superconducting devices [195].

7.6 Reducing the effects of dissipation

If all of the proposed solutions fail, there is a low tech solution: accept the dissipation, but guide the heat away from the sample. For low levels of dissipation, this can be done by covering the RF wire with a gold or copper layer with its own thermalization channels. For a 300 nm thick copper layer with a width of 300 μm and a total length of 2.5 mm we expect a thermal resistance of 3 mK/nW, where we assume the thermal conductivity to be $\sim$ 10 W/mK at 100 mK. This rough estimate is backed up by a more accurate finite element analysis of the local temperature of the RF wire for various RF powers, as can be seen in Fig. 7.11. In this analysis a power P is applied at the RF wire, which is placed on top of a silicon chip with $\kappa_{\mathrm{Si}} \propto T^3$, as expected for insulating materials [196]. The bottom of this chip is assumed to be perfectly thermalized to the sample holder.

It shows that even with very moderate dissipated powers the local temperature of the RF wire increases far above the temperature of the sample holder. Adding additional heat conductance by covering the RF wire with copper as described above is a significant improvement, and is therefore highly recommended. For the copper thermalization, we assume that the edge of the copper is properly thermalized to the sample holder, and $\kappa_{\mathrm{Cu}} \propto T$. The simulation shows that the improvement is a combined effect of direct cooling via the copper and a larger effective contact area to the silicon substrate.

Alternatively, it might be possible to keep the RF source separated from the sample, for instance by putting it on a different chip or by switching to a more

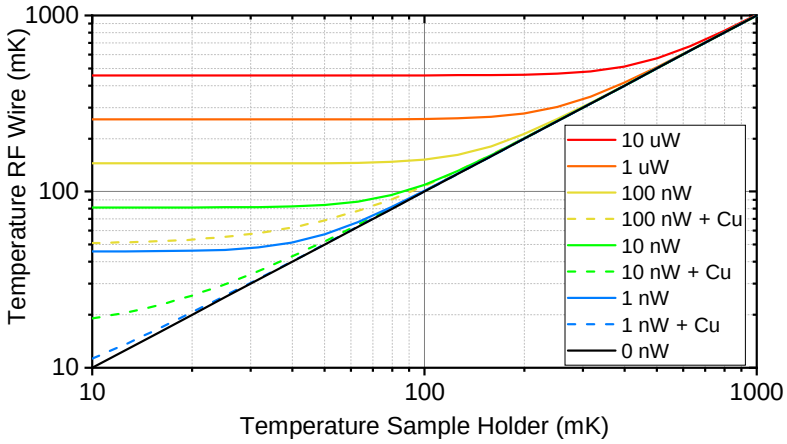

Figure 7.11: Finite element analysis of the local temperature of the RF wire while applying various powers, with and without additional copper thermalization.

long-ranged RF source. For high dissipation, this might be a better alternative, but it remains technically challenging to prevent a parasitic heat flow to the sample. Furthermore, a more long-ranged RF field would cause eddy current dissipation in surrounding metals to increase.

7.7 Conclusions

In this chapter, we have described the possibility of using Fermat as a highly sensitive calorimeter to measure the dissipation induced by the RF fields generated by the RF wire. We have measured this dissipation for various RF amplitudes and frequencies, concluding that the dissipation scales with I^2 and f^n, where n was found to vary between 1 (at low frequency) and 1.5 (at high frequency). We did not find a temperature dependence for temperatures below 500 mK. We evaluated various models for the dissipation, including eddy current losses and the intrinsic dissipation in superconductors when carrying an AC current. Our conclusion is that eddy currents only contribute to a small part of the observed dissipation, so completely removing these will only give a marginal improvement. We hypothesize that the dissipation is caused by the presence of flux vortices within the superconducting RF wire, but we were so far unable to match our data to a specific mechanism.

We have proposed some technical adjustments which might reduce the (effects of the) dissipation. When the NbTiN is indeed the source of the dissipation, we would

advise to start by fabricating detection chips with an additional thermalization of the RF wire. The gold thermalization is easy to implement, and based on the simulations it should offer a significant reduction of the sample temperature resulting from the dissipated power.

We end this chapter by calculating whether the measured dissipation allows to do an imaging experiment on protons with a B_1 field of 4 mT. At a distance of 0.5 μm from the RF wire, this requires a current of 20 mA_{pk}. The Larmor frequency of protons in a field of 100 mT is roughly 4 MHz. We extrapolate that a continuous power RF pulse with these parameters would dissipate roughly 30 - 40 μW, which would rule out continuous power protocols. Fortunately, most MRFM protocols have a low duty-cycle. For instance, cyclic-CERMIT has a duty cycle of only 0.5%, as the RF power is only switched on once every several cantilever periods [14].

Assuming that by using a properly chosen MRFM protocol, we can reduce the dissipation to 1 μW. According to the simulations in Fig. 7.11, this would allow sample temperatures close to 100 mK, which is already quite good. We can improve on this by increasing the thickness of the RF wire from 300 nm to 1 μm, as this would reduce the dissipation by an additional factor of 10 according to Eq. 7.10. The resulting 100 nW dissipation would heat the sample to about 50 mK. Therefore, based on these estimates, we are cautiously optimistic that the proposed technical improvements will reduce the dissipation from the RF wire, and enable a full fledged milliKelvin MRFM experiment.